Reaction Chemistry & Engineering

ROYAL SOCIETY OF CHEMISTRY

PAPER

View Article Online
View Journal | View Issue

Check for updates

Cite this: *React. Chem. Eng.*, 2022, 7, 908

Copper-based MOF, $Cu_3(SDBA)_2(HSDBA)$, as a catalyst for efficient reduction of 4-nitrophenol in the presence of sodium borohydride†

Manel Mansour,[ab] Hamza Kahri,*[c] Mouhieddinne Guergueb,[d] Houcine Barhoumi,[c] Enrique Gutierrez Puebla,[b] Brahim Ayed[a] and Umit B. Demirci*[e]

Received 15th November 2021,
Accepted 5th January 2022

DOI: 10.1039/d1re00506e

rsc.li/reaction-engineering

Herein, we report the synthesis of the copper-based MOF, $Cu_3(SDBA)_2(HSDBA)$, using a solvothermal method. The physicochemical properties of the as-prepared sample were examined by X-ray diffraction, scanning electron microscopy, energy-dispersive X-ray spectroscopy, Fourier-transform infrared and UV-vis spectroscopy techniques, and thermal analysis. $Cu_3(SDBA)_2(HSDBA)$ was then investigated as a catalyst for the reduction of 4-nitrophenol (4-NP) in the presence of sodium borohydride ($NaBH_4$) at 25 °C, and related kinetics and thermodynamics analyses were carried out. In a nutshell, it can be emphasized that, under our conditions, the $Cu_3(SDBA)_2(HSDBA)$ catalyst is able to completely reduce 4-NP to 4-aminophenol (4-AP) in a very short time such as 20 s. Additionally, $Cu_3(SDBA)_2(HSDBA)$ can be re-used for seven successive cycles without obvious change in its catalytic activity.

1. Introduction

Nitroaromatic compounds such as nitrophenols are important intermediates for industrial applications including pharmaceuticals, leather, plastics, fungicides, pesticides and insecticides.[1–5] Nevertheless, some nitrophenols such as 4-nitrophenol (4-NP) are hazardous as they cause eye inflammation, skin allergies and respiratory problems.

It is therefore important to remove 4-NP from aqueous solution. Different methods have been reported, and these methods cover adsorption, photocatalytic degradation, microwave-assisted catalytic oxidation and electro-Fenton.[6–11] The catalytic reduction of 4-NP to 4-aminophenol (4-AP) has also been described. A variety of catalysts were reported for this reaction.[12–18] These catalysts provide high efficiency and high recyclability, as is the case with N-doped reduced graphene metal oxide nanocomposites for example.[19–21] Metal–organic frameworks (MOFs) are a class of hybrid porous materials, displaying high surface areas and tunable pore size/volume.[22] MOFs, specifically catalytic nanoparticles supported on MOFs, can be used as catalysts for the reduction of 4-NP to 4-AP. Examples are as follows: nanoparticles of Ni@Pd supported on UiO-66-NH_2,[23] and Cu-based 2D MOFs.[24] MOFs were also utilized as a template for the preparation of porous carbon. Examples are as follows: nanoparticles of Co supported on a porous carbon stemming from carbonization of benzene-1,4-dicarboxylic acid-based MOFs,[25] and a comparable supported catalyst where the nanoparticles were made of Fe.[26] Such MOF-based catalysts offer advantages such as high catalytic performance, as well as drawbacks such as lack of stability. Thus, it is important to further explore MOF-based catalysts showing excellent performance in terms of kinetics and very good stability for the reduction of 4-NP to 4-AP in aqueous solution and under mild conditions.

In this study, we report the synthesis of the copper-based MOF $Cu_3(SDBA)_2(HSDBA)$ using a solvothermal method where 4,4′-sulfonyldibenzoic acid (H_2-SDBA) is used as a precursor. The as-prepared catalyst was characterized employing various techniques such as SEM-EDX, FTIR, XRD, UV-vis and TGA-DSC. Our catalyst showed high efficiency as well as very good stability towards the reduction of 4-NP using sodium borohydride $NaBH_4$ as a reducing agent.

[a] *Laboratory Materials, Crystal Chemistry and Applied Thermodynamics, Faculty of Sciences of Monastir, University of Monastir, Monastir, Tunisia*
[b] *Materials Science Factory, Materials Science Institute of Madrid (CSIC), C/Sor Juana Ines de La Cruz, 3, Madrid, Spain*
[c] *Laboratory of Interfaces and Advanced Materials, Faculty of Sciences, University of Monastir, Tunisia. E-mail: kahrihamza11@gmail.com*
[d] *University of Monastir, Laboratoire de Physico-Chimie des Matériaux, Faculté des Sciences de Monastir, Avenue de l'Environnement, 5019 Monastir, Tunisia*
[e] *IEM (Institut Européen des Membranes), UMR5635 (CNRS, ENSCM, UM), Université de Montpellier, Place Eugene Bataillon, CC047, Montpellier, France. E-mail: umit.demirci@umontpellier.fr*

† Electronic supplementary information (ESI) available. See DOI: 10.1039/d1re00506e

2. Methodology

2.1. Synthesis method

$Cu_3(SDBA)_2(HSDBA)$ was synthesized under hydrothermal conditions as follows (Fig. S1†). Copper nitrate trihydrate $Cu(NO_3)_2{\cdot}3H_2O$ (0.5 mmol; 99%; Sigma-Aldrich) and 4,4′-sulfonyldibenzoic acid $C_{14}H_{10}O_6S$ (0.5 mmol; denoted H_2-SDBA; 98%; Sigma-Aldrich) were dissolved in 5 mL of deionized water (resistivity >18.2 MΩ cm). The solution was transferred in a Teflon vessel (25 mL) that was sealed and placed in a stainless-steel autoclave. Then, the autoclave was placed in an oven preheated at 170 °C, and kept there for 3 days. It is worth mentioning that the time was optimized; the crystals with the best quality formed after 3 days. After cooling to room temperature, the as-obtained blue crystals of $Cu_3(SDBA)_2(HSDBA)$ were filtered off and washed with water, ethanol and acetone.

2.2. Characterization methods

$Cu_3(SDBA)_2(HSDBA)$ was scrutinized by scanning electron microscopy (SEM) and its chemical composition was analyzed by electron dispersive X-ray spectroscopy (EDS). An S-3000N microscope equipped with an ESED and an INCAX-sight from Oxford Instruments was used. The samples to be analyzed were prepared as follows. $Cu_3(SDBA)_2(HSDBA)$ was dispersed onto a double-sided adhesive conductive carbon tape that was attached to a flat aluminum sample holder, and it was metalized using a 12 nm gold layer with a Quorum Q150T-S sputter.

Elemental analysis was performed using a PerkinElmer2400 CHN elemental analyzer.

Molecular analysis of $Cu_3(SDBA)_2(HSDBA)$ was performed by Fourier-transform infrared spectroscopy (Perkin-Elmer spectrophotometer). A thin transparent pellet was made by compacting an intimate mixture of 2 mg of $Cu_3(SDBA)_2(HSDBA)$ and 100 mg of potassium bromide KBr (99%; Sigma-Aldrich). The spectrum was recorded at 45 scans per minute at room temperature from 4000 to 400 cm^{-1}.

Structural analyses of $Cu_3(SDBA)_2(HSDBA)$ were carried out. In a first step, single crystal XRD experiment was performed upon selection of $Cu_3(SDBA)_2(HSDBA)$ crystals using a polarized optical microscope. Single-crystal X-ray data were collected using a Bruker four-circle kappa diffractometer equipped with a Cu INCOATED micro-source, operated at 30 W (45 kV, 0.60 mA) to generate Cu Kα radiation (λ = 1.54178 Å), and with a Bruker VANTEC-500 detector (micro-gap technology). The diffraction data were collected, exploring over the reciprocal space in a combination of f and w scans to reach a resolution of 0.85 Å, with a completeness >95% and a redundancy >3. For this purpose, a generic hemisphere collection strategy has been developed using Bruker APEX3 and the software suite was used.[27] The exposure time was adjusted on the basis of the size and diffraction quality of the specimens, each exposure covering 1° in ω or φ. Unit cell dimensions were determined for least-squares fit of reflections with $I > 4$ s. The structures were solved by direct methods implemented in the SHELX package.[28] The hydrogen atoms were fixed at their calculated positions using distances and angle constraints. All calculations were performed using APEX3 software for data collection, and OLEX2-1.2 (ref. 29) and SHELXTL28 to resolve and refine the structure. All non-hydrogen atoms were anisotropically refined. In a first step, powder X-ray diffraction (PRXD) data were collected. The PRXD patterns were measured using a Bruker D8 diffractometer with a Cu source operated at 1600 W, with a step size of 0.02° and an exposure time of 0.5 s per step. The PXRD measurements were used to check the purity of the obtained microcrystalline product by comparison of the experimental results with the calculated pattern obtained from the single-crystal XRD data.

The solid-state UV-vis spectra of $Cu_3(SDBA)_2(HSDBA)$ and of the ligand H_2-SDPA were obtained at room temperature using a Perkin-Elmer Lambda 950 spectrometer within a 200–800 nm wavelength range. The spectra allowed the determination of the gap energy E_{gap} (in eV) that is defined as the difference between the energy level of the highest occupied molecular orbital (E_{HOMO}) and the energy level of the lowest unoccupied molecular orbital (E_{LUMO}):

$$E_{gap} = E_{HOMO} - E_{LUMO} = h\nu = \frac{hc}{\lambda_{lim}} \quad (1)$$

with h the Planck's constant, c the speed of light in a vacuum, and λ_{lim} the wavelength of the photon (nm). E_{gap} corresponds then to the lowest transition optical energy that the material could be absorbed, and such an optical band gap (in eV) can be calculated using the equation:

$$E_{gap} = \frac{1241}{\lambda_{lim}} \quad (2)$$

Thermogravimetric (TG) and differential scanning calorimetry (DSC) analyses were performed with a NETZSCHSTA 449 F3 simultaneous thermal analyzer under a N_2 atmosphere at a heating rate of 10 °C min^{-1} over a temperature range of 31 to 900 °C using an open platinum crucible. The sample weight used was about 4 mg.

2.3. Catalytic reduction of 4-nitrophenol

A 5 mL aqueous solution containing 2.1×10^{-2} mol of sodium borohydride $NaBH_4$ (96%; Sigma-Aldrich) and 7.1×10^{-4} mol of 4-nitrophenol (4-NP; 99%; Sigma-Aldrich) was prepared. To start the reduction reaction, 2 mg of $Cu_3(SDBA)_2(HSDBA)$ was added to the solution. To follow the reduction of 4-NP, absorbance values at 400 nm were recorded using a UV-vis spectrometer (Varian Cary 5000 spectrophotometer; Agilent Technologies). The experiment was repeated at various temperatures (25, 35, 45 and 55 °C) to see the effect of the temperature and determine the apparent activation energy of the reaction under our conditions.

3. Results and discussion

3.1. Morphological and molecular analyses of $Cu_3(SDBA)_2(HSDBA)$

$Cu_3(SDBA)_2(HSDBA)$ consists of blue crystals (Fig. S1†), in fact polyhedra of various sizes. There are polyhedra of dozens of micrometers (up to 130 μm; Fig. 1a and b and S2a†), as well as smaller particles located on the facets of the bigger ones (Fig. 1c, and S2b†). Upon SEM observation, the sample was analyzed by EDS and the presence of both Cu and S was detected (Fig. S3†). These two elements were quantified by elemental analysis, with 43 and 8.4 wt% in good agreement with the calculated contents (46.4 and 8.8 wt%). Two other elements, H and N, were found, with 2.9 and 0.02 wt% respectively (*versus* 2.2 and 0 wt% for the calculated values).

The FT-IR spectra of $Cu_3(SDBA)_2(HSDBA)$ and the ligand H_2-SDBA are highly comparable (Fig. 2) in terms of the bands at 3470–3460 cm^{-1} (O–H stretching), 3100–2600 cm^{-1} (C–H aliphatic and aromatic stretching), 1700 cm^{-1} (C═O stretching), 1588–1584 cm^{-1} (O–H deformation), 1570–1429 cm^{-1} (COO asymmetric and symmetric stretching), 1289–1166 cm^{-1} (C–SO_2–C asymmetric and symmetric stretching), 1101–1019 cm^{-1} (C–C and C–O stretching), and 750–576 cm^{-1} (C–S deformation).[30,31] The spectrum of H_2-SDBA shows another band peaking at 937 cm^{-1} due to aromatic ring deformation and C–S stretching; this band cannot be seen in the spectrum of $Cu_3(SDBA)_2(HSDBA)$, which may indicate bonding between the ligands and the metal nodes. The spectrum of $Cu_3(SDBA)_2(HSDBA)$ shows an additional band, peaking at 519 cm^{-1} and corresponding to the vibrational signal of Cu–O,[32] thereby confirming the formation of $Cu_3(SDBA)_2(HSDBA)$ *via* Cu–O bonds between the metal nodes and the organic ligands.

3.2. Crystallinity of $Cu_3(SDBA)_2(HSDBA)$

The single crystal XRD analysis reveals that $Cu_3(SDBA)_2(HSDBA)$ is a 3D coordination polymer crystallizing in the triclinic crystal system, with the $P\bar{1}$ space group (Table S1†). The asymmetric unit of $Cu_3(SDBA)_2(HSDBA)$ consists in 2 $SDBA^{2-}$ anions, 1 $H\text{-}SDBA^-$ anion and 3 Cu(II) cations (Fig. 3a). The structural arrangement of $Cu_3(SDBA)_2(HSDBA)$ is shown in Fig. 3b along the [010] plane. The structure may be described as clusters (Cu_3O_{14}) made of three polyhedra with shared apices which are linked by $SDBA^{2-}$ anions. All of these dual strings run in parallel with each other. The carboxylate groups of $SDBA^{2-}$ are connected to Cu(II) in two ways: a bis-tetradentate form results in a diamond shape in the Cu_2O_{10} cluster system, and the $SDBA^{2-}$ ligands take a bridging coordination mode μ_6-COO^-. Each 1D single chain string has microporous cavities with sizes of approximately 12.82(2) and 11.6(3) $Å^2$ for Cu···Cu and S···S respectively, and one possesses a 1D related square plane geometry along the crystallographic *a*-axis (Fig. 3c).

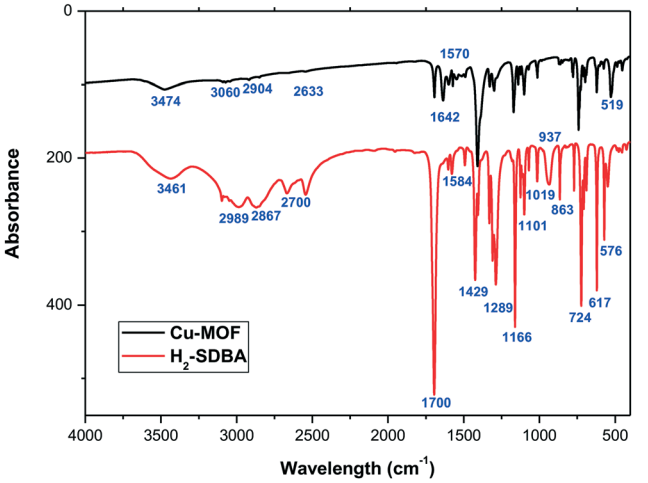

Fig. 2 FTIR spectra of $Cu_3(SDBA)_2(HSDBA$ (denoted as Cu-MOF) and H_2-SDBA.

The phase purity of bulk $Cu_3(SDBA)_2(HSDBA)$ (blue precipitate) was examined by PXRD study. The PXRD pattern shows sharp peaks showing high crystallinity (Fig. S4†). In addition, the Bragg peak positions of the PXRD pattern match well with those of the pattern calculated from the single crystal XRD data, which indicates the successful synthesis of a pure phase of $Cu_3(SDBA)_2(HSDBA)$. There is nevertheless the presence of a small amount of CuO (peak at *ca.* 35° due to the (111) plane; JCPDS: card no. 48-1548).

3.3. UV-VIS analysis of $Cu_3(SDBA)_2(HSDBA)$

The UV-vis absorption spectra of $Cu_3(SDBA)_2(HSDBA)$ and the H_2-SDBA ligand were recorded in the solid state from 200 to 800 nm. The spectrum of H_2-SDBA (Fig. S5†) exhibits two strong absorption bands with the maximum being below 300 nm (*i.e.* λ_{max} = 217 nm and λ_{max} = 292 nm), which may be contributed by the n–π* transition as well as the π–π*

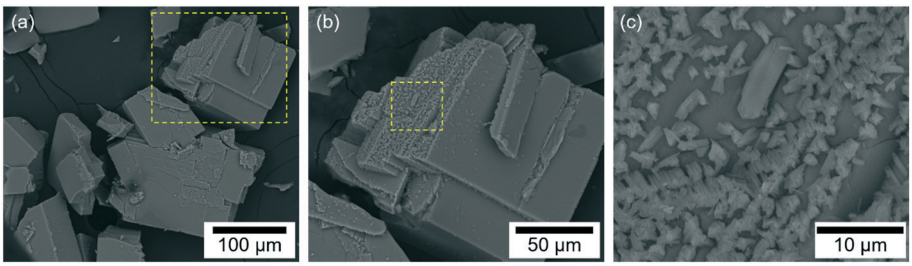

Fig. 1 SEM images of $Cu_3(SDBA)_2(HSDBA)$ at three different magnifications. Image (b) shows a magnification of the area of image (a) indicated by the yellow box. Image (c) is a magnification of the surrounding area of image (b).

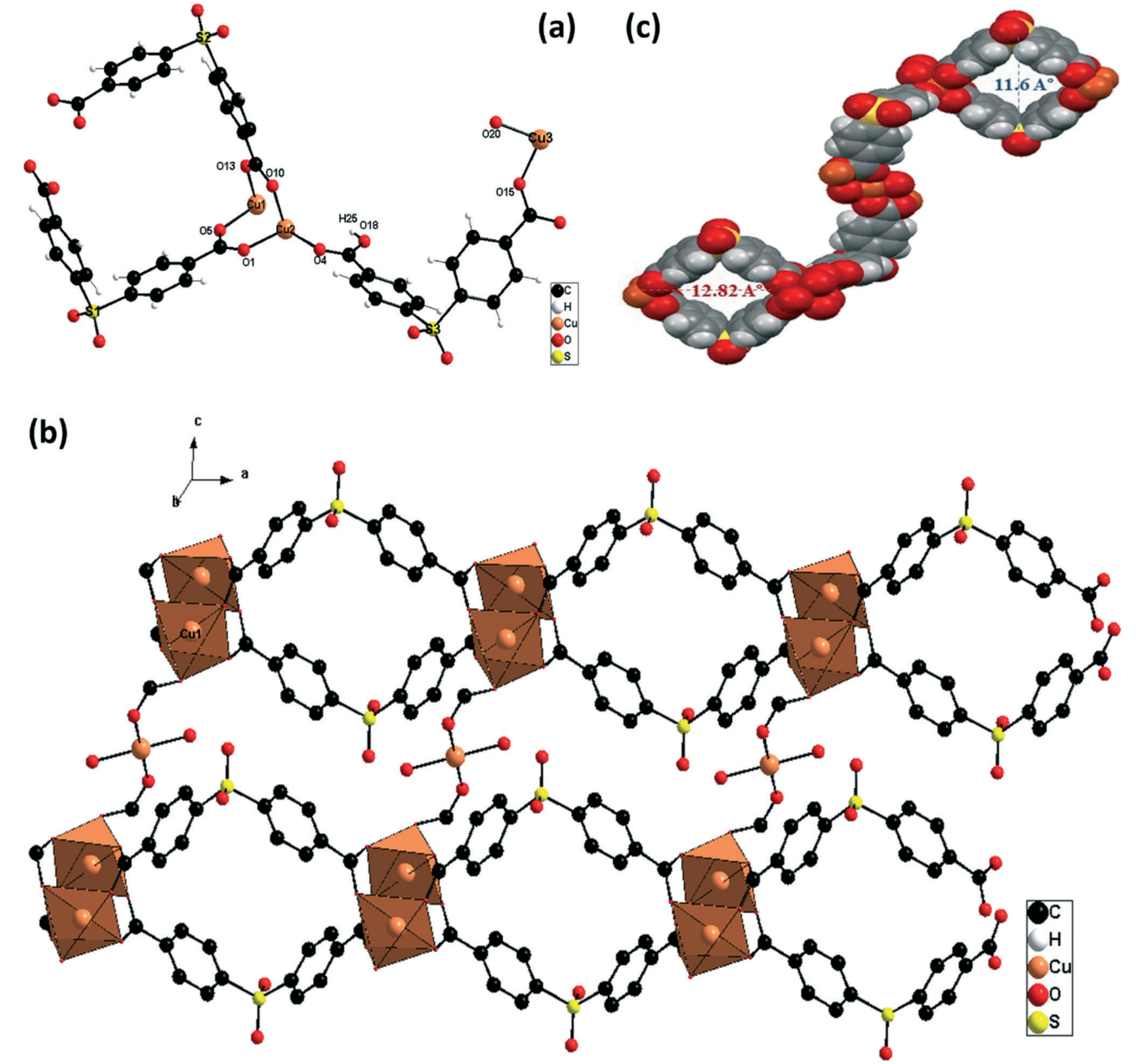

Fig. 3 (a) Asymmetric unit for $Cu_3(SDBA)_2(HSDBA)$. (b and c) Polymer coordination geometry for the ligand $SDBA^{2-}$ with Cu(II) metal centers.

transition of the aromatic rings, respectively.[33] This value corresponds to λ_{lim} at 379 nm and the energy gap (E_{gap} = 3.27 eV). This may classify the ligand as a semiconductor.[34] The UV-vis absorption spectrum of $Cu_3(SDBA)_2(HSDBA)$ (Fig. 4) shows a large band that corresponds to the charge transfer from O of the ligand to Cu.[35] The energy gap, calculated on the basis of λ_{lim} of $Cu_3(SDBA)_2(HSDBA)$, was found to be 2.13 eV, which allows classifying $Cu_3(SDBA)_2(HSDBA)$ as a semiconductor.[36]

3.4. Thermal stability of $Cu_3(SDBA)_2(HSDBA)$

TG and DSC analysis were carried out to check the thermal stability of $Cu_3(SDBA)_2(HSDBA)$ (Fig. 5). $Cu_3(SDBA)_2(HSDBA)$ is stable up to 200 °C, and above this temperature, it overcomes five successive weight losses up to about 486 °C. The first weight loss of 5.9 wt% is indicated by an endothermic signal peaking at 223 °C. This is due to the desorption of water incorporated into the pores of $Cu_3(SDBA)_2(HSDBA)$. Then, the next four weight losses (41 wt%) are associated with four exothermic signals peaking at 322, 391, 411 and 486 °C. These indicate a stepwise decomposition of the ligand.[37] Between 493 and about 650 °C, the solid is stable, and it overcomes an additional weight loss of 8 wt% up to about 750 °C. One may thus conclude that $Cu_3(SDBA)_2(HSDBA)$ is thermally stable up to 200 °C.

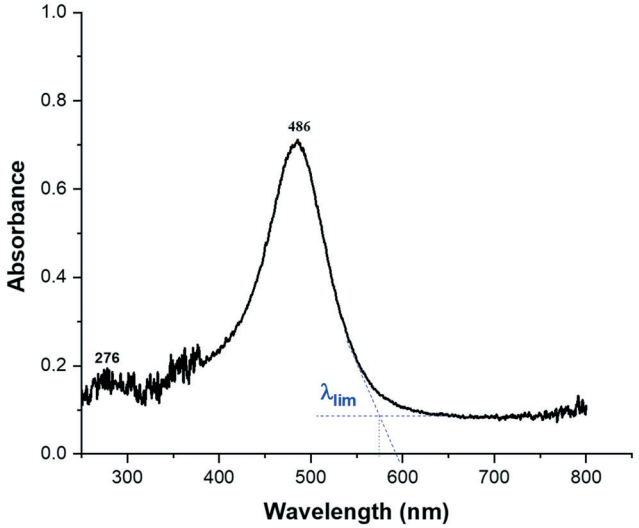

Fig. 4 UV-vis absorption spectrum of $Cu_3(SDBA)_2(HSDBA)$, where λ_{max} and λ_{lim} are indicated.

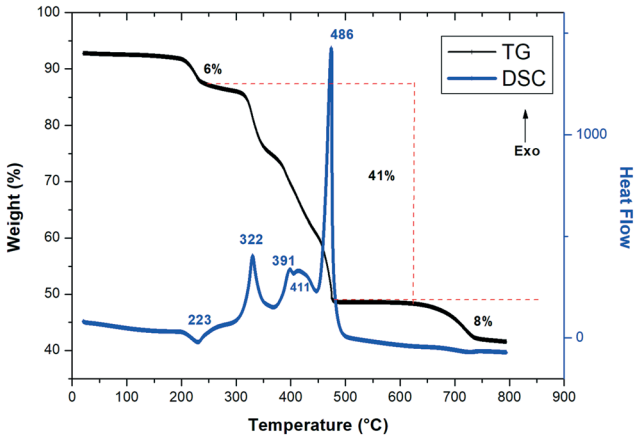

Fig. 5 TG and DSC analyses of $Cu_3(SDBA)_2(HSDBA)$.

3.5. Catalytic reduction of 4-nitrophenol

$Cu_3(SDBA)_2(HSDBA)$ was used for the reduction of 4-NP in the presence of $NaBH_4$ in aqueous solution (30-fold excess of $NaBH_4$ over 4-NP). 4-NP has an adsorption maximum at 400 nm in the reaction mixture, and its reduction was followed by monitoring the decrease of the absorption band as a function of time by UV-vis spectrophotometry. Concomitantly, a new band appeared, at 300 nm, evidencing the presence of 4-AP as the reduction product of 4-NP (Fig. 6). Under our conditions, and at 25 °C (Fig. 7), the reduction of 4-NP started upon the addition of $Cu_3(SDBA)_2(HSDBA)$ and it was totally reduced in 20 seconds. This catalytic performance may be compared to some state-of-the-art MOF-based catalysts (Table 1).[24,38–41] Under roughly similar conditions, $Cu_3(SDBA)_2(HSDBA)$ is as efficient as Pd@Co-MOF[40] for reducing 4-NP in 20 seconds; however, our $Cu_3(SDBA)_2(HSDBA)$ is free of a hydrogenation metal like Pd. It is difficult to further discuss the performance of the listed catalysts because of discrepancies in the reaction conditions,

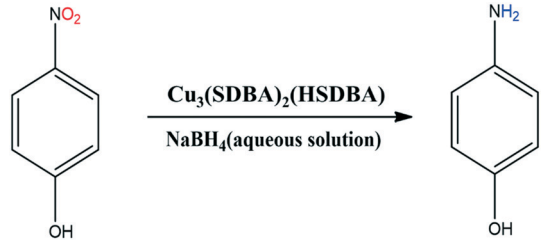

Fig. 6 Reduction of 4-nitrophenol (4-NP) to 4-aminophenol (4-AP).

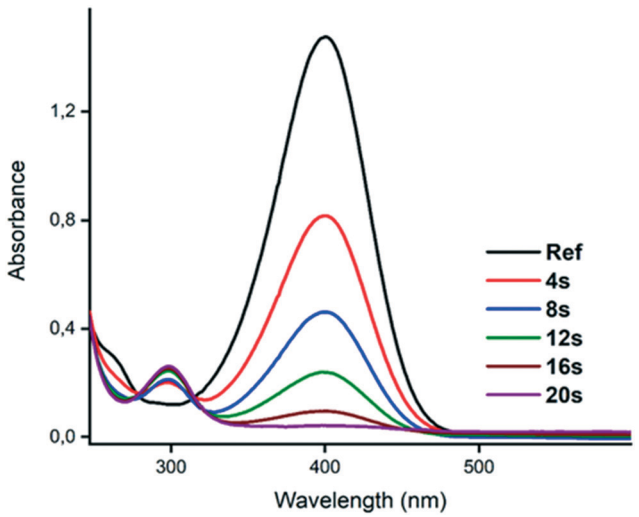

Fig. 7 UV-vis spectra of the reduction of 4-NP by $Cu_3(SDBA)_2(HSDBA)$ in aqueous $NaBH_4$ at different times (from 4 to 20 seconds). The spectrum denoted as 'Ref' is the one monitored before the addition of the $Cu_3(SDBA)_2(HSDBA)$ catalyst. Conditions: 5 mL; [4-NP] = 7.1×10^{-4} mol L^{-1}; [$NaBH_4$] = 2.1×10^{-2} mol L^{-1}; 2 mg $Cu_3(SDBA)_2(HSDBA)$; 25 °C.

but it is reasonable to observe that $Cu_3(SDBA)_2(HSDBA)$ is highly efficient in quickly reducing 4-NP at 25 °C.

Fig. 8a shows the decrease in the concentration of 4-NP (C_t/C_0) at 25 °C, as well as three other temperatures such as 35, 45 and 55 °C, as a function of time. The curves were exploited to plot $-\ln(C_t/C_0)$ as a function of time, as shown in Fig. 8b. There is a good linear correlation, thereby confirming that the reduction of 4-NP is consistent with first-order reaction kinetics.[42] This allowed us to calculate the pseudo-first order rate constants k that were found to be 0.25, 0.31, 0.34 and 0.36 s^{-1} at 25, 35, 45 and 55 °C, respectively.

The activation and thermodynamic parameters for the reduction of 4-NP by $Cu_3(SDBA)_2(HSDBA)$ were calculated using the Arrhenius and Eyring equations:

$$\ln(k) = \ln(A) - \frac{E_a}{RT} \quad (3)$$

$$\ln\left(\frac{k}{T}\right) = \ln\left(\frac{k_B}{h}\right) + \frac{\Delta S^*}{R} - \frac{\Delta H^*}{RT} \quad (4)$$

where E_a is the apparent activation energy (J mol^{-1}), A is the pre-exponential factor, R is the ideal gas constant (8.314 J K^{-1}

Table 1 Comparison of $Cu_3(SDBA)_2(HSDBA)$ to state-of-the-art MOF-based catalysts for the reduction of 4-NP. The catalyst weight, the concentrations in 4-NP and $NaBH_4$, the reaction temperature, the conversion and the related time are given

Catalyst	Weight mg	[4-NP] mmol L^{-1}	[$NaBH_4$] mmol L^{-1}	Temp. °C	Conv. %	Time s	Ref.
Au@FMOF[a]	1.5	7.2	500	50	100	200	38
Ag@MOF-199/CCFs[b]	—[e]	0.1	10	25	91	600	39
Pd@Co-MOF	5	2	48	25	90	20	40
Cu_2O/Cu-MOF/rGO[c]	1	0.1	100	25	100	120	41
Cu-BDC[d]	5	0.1	100	25	100	120	24
$Cu_3(SDBA)_2(HSDBA)$	2	0.7	21	25	100	20	This study

[a] FMOF for ferrocene based metal–organic framework. [b] CCFs for carboxymethylated cellulose fibers. [c] rGO for reduced graphene oxide. [d] BDC for benzene-1,4-dicarboxylic acid. [e] Used in the form of membrane.

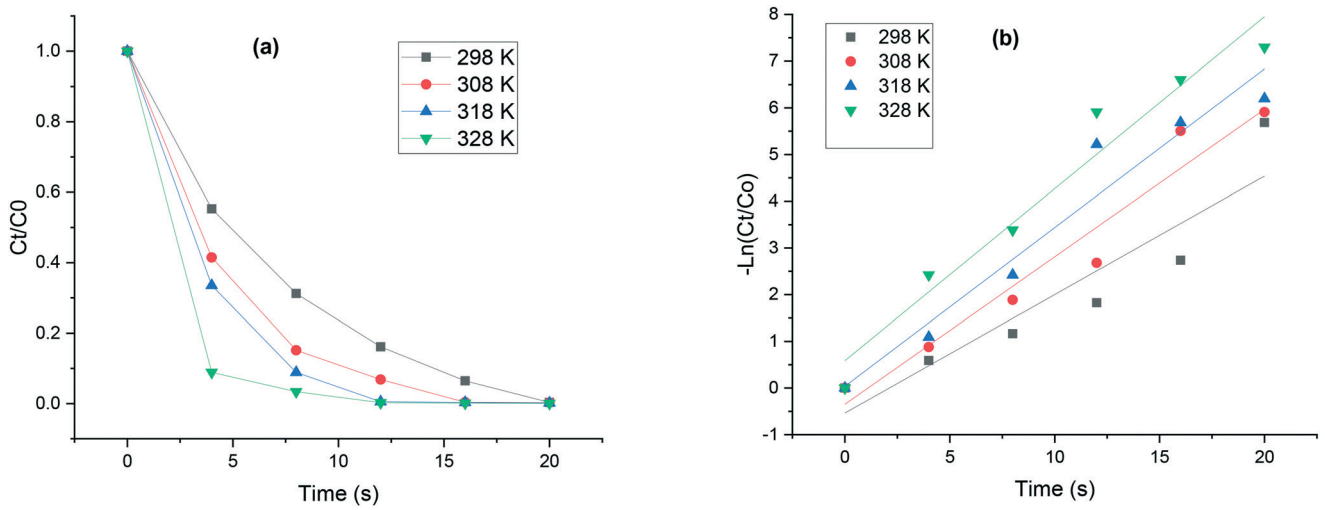

Fig. 8 (a) Change in the concentration of 4-NP (C_t/C_0) with time due to its reduction by $Cu_3(SDBA)_2(HSDBA)$ in the presence of aqueous $NaBH_4$, and (b) evolution of $-\ln(C_t/C_0)$ as a function of time. Conditions: 5 mL; [4-NP] = 7.1×10^{-4} mol L^{-1}; [$NaBH_4$] = 2.1×10^{-2} mol L^{-1}; 2 mg $Cu_3(SDBA)_2(HSDBA)$; 25, 35, 45 or 55 °C.

mol^{-1}), T is the absolute temperature (K), k_B is the Boltzmann constant (1.381×10^{-23} J K^{-1}), h is the Planck constant (6.626×10^{-34} J s), ΔS^* is the activation entropy (J mol^{-1} K^{-1}), and ΔH^* is the activation enthalpy (kJ mol^{-1}). The evolution of $\ln(k)$ as a function of $1/T$ and that of $\ln(1/k)$ as a function of $1/T$ were plotted (Fig. 9).[43] The apparent activation energy

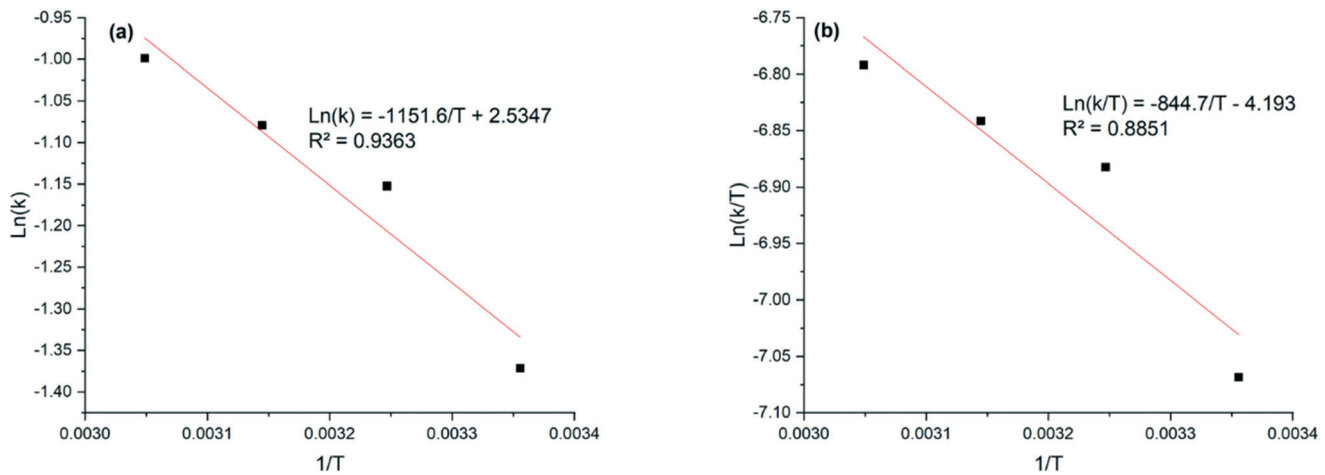

Fig. 9 (a) Evolution of $\ln(k)$ as a function of $1/T$ for the determination of the apparent activation energy. (b) Evolution of $\ln(k/T)$ as a function of $1/T$ for the determination of the thermodynamic parameters ΔS^* and ΔH^*. Conditions: 5 mL; [4-NP] = 7.1×10^{-4} mol L^{-1}; [$NaBH_4$] = 2.1×10^{-2} mol L^{-1}; 2 mg $Cu_3(SDBA)_2(HSDBA)$; 25, 35, 45 and 55 °C.

was found as E_a = 9.7 kJ mol^{-1}. This is one of the lowest values reported for the reduction of 4-NP with respect to other catalysts, and it evidences the effective catalytic activity of $Cu_3(SDBA)_2(HSDBA)$. For example, the E_a reported for ionic liquid-stabilized gold nanoparticles is 99.4 kJ mol^{-1};[44] a similar apparent activation energy was reported for a Pt–Pd alloy.[45] With respect to the activation enthalpy of $Cu_3(SDBA)_2(HSDBA)$, it was found to be ΔH^* = 7.0 kJ mol^{-1}.[46] Higher enthalpies of 97 and 110 kJ mol^{-1} were reported for ionic liquid-stabilized gold nanoparticles[44] and palladium nanoparticles,[47] respectively. The activation entropy of $Cu_3(SDBA)_2(HSDBA)$ was determined to be ΔS^* = 232.4 J mol^{-1} K^{-1}. The activation entropy is positive, which may signify a dissociative mechanism.[44,47]

The recyclability of $Cu_3(SDBA)_2(HSDBA)$ for the reduction of 4-NP was studied. To do this, after each cycle, the spent solution was filtered by centrifugation (3500 rpm, 10 min); most of the filtrate was removed and the remaining solid was washed with water and ethanol (with intermediate centrifugation); the washed solid was then dried at 80 for 1 h; finally, the as-recovered $Cu_3(SDBA)_2(HSDBA)$ was re-used for another cycle by recharging with the reactants. Seven cycles were performed (Fig. 10 and S6†). Under our conditions, $Cu_3(SDBA)_2(HSDBA)$ is relatively stable: it exhibits a conversion of 97% after the seventh cycle, and the time of reaction slightly increases from 20 s for the first cycle to 25 s for the sixth and seventh cycle. This is comparable to the stability performance of Ag-nanoparticle-embedded FeO_3-O_4@MIL-100(Fe)[48] and better than that of Ag nanoparticles immobilized onto MOF-199 supported by carboxymethylated cellulose fibers.[39] One may however mention that Cu-BDC is fully stable over 5 cycles when used under more favorable conditions (see Table 1). In sum, $Cu_3(SDBA)_2(HSDBA)$ is active for the reduction of 4-NP in 20 seconds at 25 °C (under our conditions) and it is able to maintain 97% of its initial performance in terms of conversion after 7 successive uses. $Cu_3(SDBA)_2(HSDBA)$ thus positions itself as one of the most efficient catalysts for the catalytic reduction of 4-NP in the presence of $NaBH_4$.

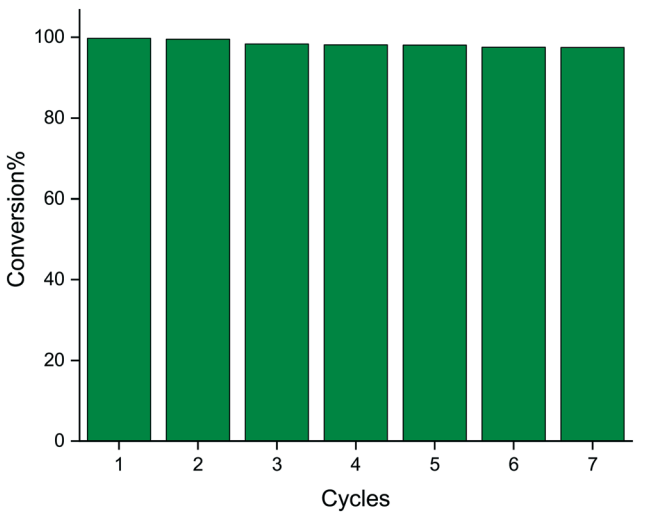

Fig. 10 Conversion of 4-NP catalyzed by re-used $Cu_3(SDBA)_2(HSDBA)$ in the presence of aqueous $NaBH_4$, for 7 cycles. Conditions: 5 mL; [4-NP] = 7.1 × 10^{-4} mol L^{-1}; [$NaBH_4$] = 2.1 × 10^{-2} mol L^{-1}; 2 mg $Cu_3(SDBA)_2(HSDBA)$; 25 °C.

$Cu_3(SDBA)_2(HSDBA)$ recovered after the aforementioned 7 cycles of use (it is now called 'used $Cu_3(SDBA)_2(HSDBA)$') was analyzed by FTIR and XRD. The FTIR spectrum (Fig. S7†) of used $Cu_3(SDBA)_2(HSDBA)$ is comparable to that of $Cu_3(SDBA)_2(HSDBA)$ (Fig. 2), except for one signal at about 1500 cm^{-1}. This could be explained by the reduction of C═O of the ligand to C–O–H by $NaBH_4$.[49] The PXRD pattern of used $Cu_3(SDBA)_2(HSDBA)$ (Fig. S8†) is different from that of $Cu_3(SDBA)_2(HSDBA)$ (Fig. S7†). This shows only the diffraction peak at about 43.5°, which is ascribed to the (111) plane of metallic Cu, formed by reduction of CuO ((111) plane) by $NaBH_4$. Otherwise, used $Cu_3(SDBA)_2(HSDBA)$ is amorphous, and the presence of one or more amorphous phases could be explained by the agglomeration of the $Cu_3(SDBA)_2(HSDBA)$ particles.[50] These changes are in line with the slight evolution of the catalytic activity of $Cu_3(SDBA)_2(HSDBA)$ after 7 cycles.

4. Conclusion

$Cu_3(SDBA)_2(HSDBA)$ has been successfully prepared using a solvothermal method. Its purity and morphology were examined by different techniques such as XRD, SEM-EDS, FTIR, UV-vis and TGA-DSC. Under our conditions, $Cu_3(SDBA)_2(HSDBA)$ has a high catalytic performance for the reduction of 4-NP to 4-AP in the presence of $NaBH_4$ at 25 °C: indeed, the reduction of 4-NP started upon the addition of $Cu_3(SDBA)_2(HSDBA)$ and 4-NP was totally reduced in 20 seconds. The activation energy, activation enthalpy, and activation entropy, which were all determined through a systematic study, are of 9.7 kJ mol^{-1}, 7.0 kJ mol^{-1}, and 232.4 J mol^{-1} K^{-1}, respectively. $Cu_3(SDBA)_2(HSDBA)$ was also assessed for re-use over several successive cycles, and it has shown very good stability; it typically kept 97% of its initial performance in terms of conversion after seven cycles. $Cu_3(SDBA)_2(HSDBA)$ is thus a suitable catalyst for the reduction of 4-NP to 4-AP in the presence of $NaBH_4$ at 25 °C.

Conflicts of interest

The authors have no conflicts of interest to disclose.

Acknowledgements

This work was supported by the Tunisian National Ministry of Higher Education and Scientific Research, an Agreement of Collaboration between the University of Monastir and the Materials Science Factory, Materials Science Institute of Madrid (CSIC; C/ Sor Juana Ines de La Cruz, 3, Madrid, Spain).

References

1 T. He, C. Zhang, L. Zhang and A. Du, Single Pt atom decorated graphitic carbon nitride as an efficient photocatalyst for the hydrogenation of nitrobenzene into aniline, *Nano Res.*, 2019, **12**, 1817–1823.

2 M. M. Kgatitsoe, S. Ncube, H. Tutu, I. A. Nyambe and L. Chimuka, Synthesis and characterization of a magnetic nanosorbent modified with Moringa oleifera leaf extracts for removal of nitroaromatic explosive compounds in water samples, *J. Environ. Chem. Eng.*, 2019, **7**, 103128.

3 Y. Xu, X. Shi, R. Hua, R. Zhang, Y. Yao, B. Zhao, T. Liu, J. Zheng and G. Lu, Remarkably catalytic activity in reduction of 4-nitrophenol and methylene blue by Fe_3O_4@COF supported noble metal nanoparticles, *Appl. Catal., B*, 2020, **260**, 118142.

4 A. H. Kianfar and M. A. Arayesh, Synthesis, characterization and investigation of photocatalytic and catalytic applications of Fe_3O_4/TiO_2/CuO nanoparticles for degradation of MB and reduction of nitrophenols, *J. Environ. Chem. Eng.*, 2020, **8**, 103640.

5 F. Liu, X. Liu, D. Astruc and H. Gu, Dendronized triazolyl-containing ferrocenyl polymers as stabilizers of gold nanoparticles for recyclable two-phase reduction of 4-nitrophenol, *J. Colloid Interface Sci.*, 2019, **5**, 161–170.

6 J. N. Jebaranjitham, C. Mageshwari, R. Saravanan and N. Mu, Fabrication of amine functionalized graphene oxide-Ag NPs nanocomposite with improved dispersibility for reduction of 4-nitrophenol, *Composites, Part B*, 2019, **171**, 302–309.

7 J. Singh, A. Mehta, M. Rawat and S. Basu, Green synthesis of silver nanoparticles using sun dried tulsi leaves and its catalytic application for 4-nitrophenol reduction, *J. Environ. Chem. Eng.*, 2018, **6**, 1468–1474.

8 M. T. Nakhjiri, G. B. Marandi and M. Kurdtabar, Preparation of magnetic double network nanocomposite hydrogel for adsorption of phenol and p-nitrophenol from aqueous solution, *J. Environ. Chem. Eng.*, 2021, **9**, 105039.

9 L. L. Bo, Y. B. Zhang, X. Quan and B. Zhao, Microwave assisted catalytic oxidation of p-nitrophenol in aqueous solution using carbon-supported copper catalyst, *J. Hazard. Mater.*, 2008, **153**, 1201–1206.

10 M. Heibati, J. Elham and V. Farzaneh, Photocatalytic Degradation of p-nitrophenol in an annular volumn photoreactor and the intermediates, *Water Environ. Res.*, 2015, **87**, 437–443.

11 P. Menon, T. S. A. Singh, N. Pani and P. V. Nidheesh, Electro-Fenton assisted sonication for removal of ammoniacal nitrogen and organic matter from dye intermediate industrial wastewater, *Chemosphere*, 2021, **269**, 128739.

12 F. M. Valadi and M. R. Gholami, Synthesis of $CuCo_2O_4$/$BiVO_4$ composites as promise and efficient catalysts for 4-nitrophenol reduction in water: Experimental and theoretical study, *J. Environ. Chem. Eng.*, 2021, **9**, 105408.

13 D. Chen, L. Wu, S. Nie and P. Zhang, Solvent-free synthesis of N-doped carbon-based catalyst for high-efficient reduction of 4-nitrophenol, *J. Environ. Chem. Eng.*, 2021, **9**, 105649.

14 S. Ni, L. Yang, H. Qu, X. Zhu, Z. Xu, M. Yuan, H. Xing, L. Wang, J. Yu and H. Lu, Tailoring the structure and energy level over transition-metal doped MoS_2 towards enhancing 4-nitrophenol reduction reaction, *J. Environ. Chem. Eng.*, 2021, **9**, 105101.

15 P. Xiao, S. Wang, X. Xu and J. Zhu, In-situ template formation method to synthesize hierarchically porous carbon for electrocatalytic reduction of 4-nitrophenol, *Carbon*, 2021, **184**, 596–608.

16 F. S. Alamro, A. M. Mostafa, H. A. Ahmed and A. Toghan, Zinc oxide/carbon nanotubes nanocomposite: Synthesis, characterization and catalytic reduction of 4-nitrophenol via laser assistant method, *Surf. Interfaces*, 2021, **26**, 101406.

17 W. Shen, Y. Qu, X. Pei, S. Li, S. You, J. Wang, Z. Zhang and J. Zhou, Catalytic reduction of 4-nitrophenol using gold nanoparticles biosynthesized by cell-free extracts of Aspergillus sp. WL-Au, *J. Hazard. Mater.*, 2017, **321**, 299–306.

18 S. Jana, S. Konar, B. C. Mitra, A. Mondal and S. Mukhopadhyay, Fabrication of a new heterostructure Au/Pt/SnO_2: An excellent catalyst for fast reduction of para-nitrophenol and visible light assisted photodegradation of dyes, *Mater. Res. Bull.*, 2021, **141**, 111351.

19 M. J. S. Mohamed, U. S. Shenoy and D. K. Bhat, Enhanced photocatalytic performance of N-doped RGO-$FeWO_4/Fe_3O_4$ ternary nanocomposite in environmental applications, *Mater. Today Chem.*, 2017, **4**, 133–141.

20 M. J. S. Mohamed, U. S. Shenoy and D. K. Bhat, Novel NRGO-$CoWO_4$-Fe_2O_3 nanocomposite as an efficient catalyst for dye degradation and reduction of 4-nitrophenol, *Mater. Chem. Phys.*, 2018, **208**, 112–122.

21 M. J. S. Mohamed, U. S. Shenoy and D. K. Bhat, Synthesis of $BaWO_4$/NRGO–g-C_3N_4 nanocomposites with excellent multifunctional catalytic performance via microwave approach, *Front. Mater. Sci.*, 2018, **12**, 247–263.

22 D. Wu, P. F. Zhang, G. P. Yang, L. Hou, W. Y. Zhang, Y. F. Han and Y. Y. Wang, Supramolecular control of MOF pore properties for the tailored guest adsorption/separation applications, *Coord. Chem. Rev.*, 2021, **434**, 213709.

23 S. M. Sadeghzadeh, R. Zhiani and S. Emrani, The reduction of 4-nitrophenol and 2-nitroaniline by the incorporation of Ni@Pd MNPs into modified UiO-66-NH_2 metal–organic frameworks (MOFs) with tetrathia-azacyclopentadecane, *New J. Chem.*, 2018, **42**, 988–994.

24 H. N. Abdelhamid, High performance and ultrafast reduction of 4-nitrophenol using metal-organic frameworks, *J. Environ. Chem. Eng.*, 2021, **9**, 104404.

25 M. A. Ahsan, O. Fernandez-Delgado, E. Deemer, H. Wang, A. A. El-Gendy, M. L. Curry and J. C. Noveron, Carbonization of Co-BDC MOF results in magnetic C@Co nanoparticles that catalyze the reduction of methyl orange and 4-nitrophenol in water, *J. Mol. Liq.*, 2019, **290**, 111059.

26 M. A. Ahsan, O. Fernandez-Delgado, E. Deemer, H. Wang, A. A. El-Gendy, M. L. Curry and J. C. Noveron, Fe

nanoparticles encapsulated in MOF-derived carbon for the reduction of 4-nitrophenol and methyl orange in water, *Catal. Commun.*, 2019, **130**, 105753.

27 M. Y. Pan, S. Q. Xia and X. T. Tao, Crystal structure of $Ba_5In_4Sb_6$, *Acta Crystallogr., Sect. E: Crystallogr. Commun.*, 2015, **71**, i4.933.

28 L. J. Farrugia, WinGX suite for small-molecule single-crystal crystallography, *J. Appl. Crystallogr.*, 1999, **32**, 837–838.

29 G. M. Sheldrick, A short history of SHELX, *Acta Crystallogr., Sect. A: Found. Crystallogr.*, 2008, **64**, 112–122.

30 K. Y. A. Lin and Y. T. Hsieh, Copper-based metal organic framework (MOF), HKUST-1, as an efficient adsorbent to remove p-nitrophenol from water, *J. Taiwan Inst. Chem. Eng.*, 2015, **50**, 223–228.

31 U. Jamil, A. H. Khoja, R. Liaquat, S. R. Naqvi, W. N. N. W. Omar and N. A. S. Amin, Copper and calcium-based metal organic framework (MOF) catalyst for biodiesel production from waste cooking oil: A process optimization study, *Energy Convers. Manage.*, 2020, **215**, 112934.

32 R. Rani, A. Deep, B. Mizaikoff and S. Singh, Enhanced hydrothermal stability of Cu MOF by post synthetic modification with amino acids, *Vacuum*, 2019, **164**, 449–457.

33 S. Bhattacharya and S. Natarajan, Stabilization of Co_3 –oxoclusters in a pcu net: Synthesis, structure, solvent exchange (single crystal to single crystal) and magnetic studies, *Z. Anorg. Allg. Chem.*, 2014, **14**, 2922–2930.

34 J. Zhou, Y. Liu, J. Tang and W. Tang, Surface ligands engineering of semiconductor quantum dots for chemosensory and biological applications, *Mater. Today*, 2017, **20**, 360–376.

35 S. Biswas, R. Saha and A. Ghosh, Copper (II)–Mercury (II) Heterometallic complexes derived from a salen-type ligand: A new coordination mode of the old Schiff base ligand, *Organometallics*, 2012, **31**, 3844–3850.

36 Q. Q. Huang, Y. J. Lin, R. Zheng, W. H. Deng, C. Kashi, P. N. Kumar, G. E. Wang and G. Xu, Tunable electrical conductivity of a new 3D MOFs: Cu-TATAB, *Inorg. Chem. Commun.*, 2019, **105**, 119–124.

37 A. Pal, S. Chand, S. M. Elahi and M. C. Das, A microporous MOF with a polar pore surface exhibiting excellent selective adsorption of CO_2 from CO_2–N_2 and CO_2–CH_4 gas mixtures with high CO_2 loading, *Dalton Trans.*, 2017, **46**, 15280–15286.

38 J. Liu, H. Yu and L. Wang, Effective reduction of 4-nitrophenol with Au NPs loaded ultrathin two dimensional metal-organic framework nanosheets, *Appl. Catal., A*, 2020, **599**, 117605.

39 C. Duan, C. Liu, X. Meng, W. Lu and Y. Ni, Fabrication of carboxymethylated cellulose fibers supporting Ag NPs@MOF-199s nanocatalysts for catalytic reduction of 4 nitrophenol, *Appl. Organomet. Chem.*, 2019, **33**, e4865.

40 Z. Liu, L. Ning, K. Wang, L. Feng, W. Gu and X. Liu, A new cobalt metal–organic framework as a substrate for Pd nanoparticles applied in high-efficiency nitro phenol degradation and cinnamaldehyde hydrogenation, *Dalton Trans.*, 2020, **49**, 1191–1199.

41 E. Akbarzadeh, H. Z. Soheili and M. R. Gholami, Novel Cu_2O/Cu-MOF/rGO is reported as highly efficient catalyst for reduction of 4-nitrophenol, *Mater. Chem. Phys.*, 2019, **237**, 121846.

42 S. P. Shet, S. Shanmuga Priya, K. Sudhakar and M. Tahir, A review on current trends in potential use of metal-organic framework for hydrogen storage, *Int. J. Hydrogen Energy*, 2021, **46**, 11782–11803.

43 M. Guergueb, S. Nasri, J. Brahmi, F. Loiseau, F. Molton, T. Roisnel, V. Guerineau, I. Turowska-Tyrk, K. Aouadi and H. Nasri, Effect of the coordination of π-acceptor 4-cyanopyridine ligand on the structural and electronic properties of meso-tetra(para-methoxy) and meso-tetra(para-chlorophenyl) porphyrin cobalt(ii) coordination compounds, Application in the catalytic degradation of methylene blue dye, *RSC Adv.*, 2020, **10**, 6900–6918.

44 S. R. Thawarkar, B. Thombare, B. S. Munde and N. D. Khupse, Kinetic investigation for the catalytic reduction of nitrophenol using ionic liquid stabilized gold nanoparticles, *RSC Adv.*, 2018, **8**, 38384–38390.

45 M. A. Mahmoud, F. Saira and M. A. El-Sayed, Experimental evidence for the nanocage effect in catalysis with hollow nanoparticles, *Nano Lett.*, 2010, **10**, 3764–3769.

46 N. Sahiner, H. Ozay, O. Ozay and N. Aktas, A soft hydrogel reactor for cobalt nanoparticle preparation and use in the reduction of nitrophenols, *Appl. Catal., A*, 2010, **101**, 137–143.

47 A. I. Ayad, D. Luart, A. O. Dris and E. Guénin, Kinetic analysis of 4-nitrophenol reduction by "water-soluble" palladium nanoparticles, *Nanomaterials*, 2020, **10**, 1169.

48 S. Chang, C. Liu, Y. Sun, Z. Yan, X. Zhang, X. Hu and H. Zhang, Fe_3O_4 nanoparticles coated with Ag-nanoparticle-embedded metal-organic framework MIL-100(Fe) for the catalytic reduction of 4-nitrophenol, *ACS Appl. Nano Mater.*, 2020, **3**, 2302–2309.

49 D. E. Ward and C. K. Rhee, Chemsoselective reductions with sodium borohydride, *Can. J. Chem.*, 1989, **67**, 1206–1211.

50 A. Badri, S. Slimi, M. Guergueb, H. Kahri and X. Mateos, Green synthesis of copper oxide nanoparticles using Prickly Pear peel fruit extract: Characterization and catalytic activity, *Inorg. Chem. Commun.*, 2021, **134**, 109027.

